Åman, Mari; Wada, Kentaro; Matsunaga, Hisao; Remes, Heikki; Marquis, Gary

The influence of interacting small defects on the fatigue limits of a pure iron and a bearing steel

Published in:
International Journal of Fatigue

DOI:
10.1016/j.ijfatigue.2020.105560

Published: 01/06/2020

Document Version
Publisher's PDF, also known as Version of record

International Journal of Fatigue 135 (2020) 105560

Contents lists available at ScienceDirect

International Journal of Fatigue

journal homepage: www.elsevier.com/locate/ijfatigue

The influence of interacting small defects on the fatigue limits of a pure iron and a bearing steel

Mari Åman[a,*], Kentaro Wada[b,c], Hisao Matsunaga[c,d,e,f], Heikki Remes[a], Gary Marquis[a]

[a] *Department of Mechanical Engineering, School of Engineering, Aalto University, Espoo, P.O. Box 13400, FIN-00076 Aalto, Finland*
[b] *Graduate School of Engineering, Kyushu University, 744 Moto-oka, Nishi-ku, Fukuoka 819-0395, Japan*
[c] *AIST-Kyushu University Hydrogen Materials Laboratory (HydroMate), National Institute of Advanced Industrial Science and Technology (AIST), 744 Moto-oka, Nishi-ku, Fukuoka 819-0395, Japan*
[d] *Department of Mechanical Engineering, Kyushu University, 744 Moto-oka, Nishi-ku, Fukuoka 819-0395, Japan*
[e] *Research Centre for Hydrogen Industrial Use and Storage (HYDROGENIUS), Kyushu University, 744 Moto-oka, Nishi-ku, Fukuoka 819-0395, Japan*
[f] *International Institute for Carbon Neutral Energy Research (WPI-I2CNER), Kyushu University, 744 Moto-oka, Nishi-ku, Fukuoka 819-0395, Japan*

ARTICLE INFO

Keywords:
Defect interaction
Small crack
Interaction effect
Non-propagating crack
Fatigue limit

ABSTRACT

This study investigates the effect of interacting small cracks on the fatigue limits of two types of pure iron of varying strengths and of a bearing steel. The experimental results revealed that although the fatigue limits were essentially controlled by the mechanics of interacting cracks, the non-propagating crack features and the severity of crack coalescence varied greatly among the different materials. In addition, it is demonstrated that the material-independent, analytical, interaction-criterion alone is not sufficient to estimate interaction effects in reality. This research shows that the material effect can be considered in terms of hardness and non-propagating crack size.

1. Introduction

Metallic engineering components possess numerous small natural defects which could potentially become sites for fatigue crack initiation. For example, such defects may be the result of manufacturing, machining and/or surface finishing. The effect of a single small defect on fatigue strength has been comprehensively investigated in past studies [1–15]. According to a basic theory of elasticity, the sole factor to determine the fatigue limit is stress concentration factor. However, it is not crucial for controlling the fatigue limit, since in many metallic materials, the fatigue limit is defined by the non-propagation condition of cracks which have emanated from small defects. Once a crack emanates from the defect, grows till a certain length and finally becomes non-propagating, then the final state is a crack. In such a case, fatigue limit can be evaluated by fracture mechanics parameters, *i.e.* stress intensity factors, instead of stress concentrations. Therefore, a small defect can be considered to be mechanically equivalent to a small crack from the viewpoint of the fatigue limit. [1].

Although the afore-mentioned concept considers a single defect, real materials contain multiple defects that can interact if they are in close proximity. Ultimately, the occurrence of such an interaction results in a decreased fatigue limit. Defect interaction can happen under diverse circumstances, such as in the case of casting defects [1,2,4,14], weld imperfections [16–18], surface roughness [1,19–21], non-metallic inclusions [1,22–24] and so forth. In recent times, the presence of multiple defects in additively manufactured components has led to a significant reduction in their fatigue strength, consequently underscoring the importance of understanding the precise interaction effect in fatigue [25–30].

Some analytical studies of interaction problems of three-dimensional surface cracks have previously been conducted. For example, Murakami & Nemat-Nasser [31,32], Nisitani & Murakami [33], Åman [34] and Noda *et al.* [35] have evaluated stress intensity factors for interacting 3D cracks using the body force method, whereas Patel *et al.* [36] and Newman & Raju [37] have utilized finite element method. In addition, Zhu *et al.* simulated the propagation and coalescence of multiple cracks by a probabilistic method [38]. Also, experimental studies of interaction problems have been published. For instance, Li *et al.* [39] and Sonsino *et al.* [40] investigated the influence of porosity on the fatigue strength of aluminum alloys. Chen *et al.* [41], Silva *et al.* [42] and Al-Oiwaisi *et al.* [43] examined the interacting corrosion-induced cracks in pipes. Galatolo & Lazzeri [44] studied not only the interaction of two cracks but also the interaction of a crack and a circular hole, which sometimes arises in aircraft components. Deguchi

* Corresponding author.
E-mail address: mari.aman@aalto.fi (M. Åman).

https://doi.org/10.1016/j.ijfatigue.2020.105560
Received 25 November 2019; Received in revised form 19 February 2020; Accepted 20 February 2020
Available online 21 February 2020

Nomenclature

a_{NPC}	Half-length of a non-propagating crack
area	The area of the defect projected to the plane perpendicular to the maximum principal stress
$area_{eff}$	The effective area of the defect projected to the plane perpendicular to the maximum principal stress
d_i	Diameter of defect *i*
h_i	Depth of defect *i*
s	Spacing between the defects
s_{cr}	Critical spacing between the defects
HV	Vickers hardness
$K_{I,max}$	Maximum Mode I stress intensity factor
R	Stress ratio
ΔK_{th}	Threshold stress intensity factor range for a small crack
$\Delta K_{th,\ lc}$	Threshold stress intensity factor range for a long crack
σ_w	Fatigue limit
$\sigma_{w,\ exp}$	Experimentally-determined fatigue limit
$\sigma_{w,\ pred}$	Predicted fatigue limit

et al. [45] reported that the coalescence of non-propagating cracks emanating from graphite particles of a plain ductile cast iron specimen did not decrease the fatigue limit. Despite the existence of aforementioned studies, the authors are not aware of experimental works that have systematically studied the effect of interacting defects on the fatigue limit — except the previous research by authors themselves [46].

Among afore-mentioned previous researches, one of the most important analytical finding has been the concept of critical distance, *i.e.,* the space between cracks at which the interaction effect becomes negligible [32]. The *analytical critical distance* can be explained as follows: if there is sufficient space between two cracks to allow for the insertion of an additional crack of a size similar to the smaller one, the maximum Mode I stress intensity factor, $K_{I,\ max}$, is approximately equal to that of the larger crack in isolation, see Fig. 1 [1,32,34].

Since its proposal by Murakami *et al.* [47], the $\sqrt{area}$ parameter model has been widely applied for the prediction of fatigue limits influenced by small cracks or defects. The fatigue limit under a fully-reversed condition can be predicted using the $\sqrt{area}$ parameter model, as expressed by the following equation [47]:

$$\sigma_w = \frac{1.43(HV + 120)}{(\sqrt{area})^{1/6}} \tag{1}$$

where, σ_w is the fatigue limit, *HV* is the Vickers hardness and $\sqrt{area}$ is the square root of the defect area, projected to the plane perpendicular to the maximum principal stress. In order to include the effect of interaction into Eq. (1), the effective $\sqrt{area}$ is defined in consideration of the analytical critical distance (Fig. 1) [1,32,34]. Specifically, if the spacing between defects was smaller than the analytical critical distance, *i.e.*, if $s < d_2$, where *s* is the spacing between defects and d_2 is the diameter of the smaller defect, the defects were assumed from the outset to behave like a coalesced single defect, formed by the fusion of two defects with a smooth contour. Otherwise, only the area of the larger defect was taken into account in the fatigue limit prediction process.

The afore-mentioned interaction criterion was derived based on the increase in stress intensity factor(s) caused by the neighboring crack. However, this did not consider the crack growth at and below the fatigue limit, which subsequently decreases the distance between two interacting cracks, even though the cracks become non-propagating after a length of crack growth. Such a fact can lead to a discrepancy between the *analytical* critical distance and the *real* critical distance, which can only be determined experimentally. Therefore, in order to establish a comprehensive rule of interaction, empirical verification of existing criteria is necessary for various materials.

With respect to the validity of the $\sqrt{area}$ parameter model, this study provisionally explores the effect of defect interaction on the fatigue limits in diverse materials. The new experimental results relative to pure irons and a bearing steel all complement previous research involving medium carbon steel [46]. It had been concluded that the materials microstructure influenced the interaction effect primarily via the characteristics of non-propagating cracks. In order to elucidate the material outcomes, several data from the existing literature were also analyzed in support of suggestions advanced in this study. It is evident that the analytical and material-independent interaction criteria (see also BSI standard [48]) are on their own insufficient for the prediction of interaction phenomena and their real-life influence on fatigue strength.

2. Experimental procedures

2.1. Materials

The materials investigated were pure iron JIS-SUY1, hereafter referred to as SUY1, and bearing steel JIS-SUJ2, henceforth labeled as SUJ2. Since the *HV* of the as-received SUY1 (*HV* = 165) was close to the *HV* of a previously-examined, medium-carbon steel, JIS-S45C [46], henceforward identified as S45C (*HV* = 186), some SUY1 specimens were annealed to obtain a lower *HV*. Specimens were annealed at 600 °C for one hour, followed by furnace-cooling at room temperature. The resulting *HV* was 110. In order to distinguish the differently heat-treated SUY1 specimens, annealed SUY1 specimens are hereafter labeled as A-SUY1 and non-annealed ones as NA-SUY1. Initially, the SUJ2 was heat-treated at 840 °C for one hour in a deoxidizing gas, then subsequently oil-quenched and tempered at 240 °C for two hours to obtain the *HV* of 710. The microstructures of all investigated materials are displayed in Fig. 2. Fig. 2 (a) and (b) illustrate that the grain size of SUY1 remains the same both before and after annealing. Fig. 2 (c) shows that SUJ2 had typical martensitic microstructure including precipitated carbides around 10 µm in diameter. Tables 1 and 2 document the mechanical properties and chemical compositions of the materials, respectively.

2.2. Specimens and artificial defects

The specimen geometry is exhibited in Fig. 3. The gage-section surface was mirror-polished with a diamond paste in the case of SUY1 and electro-polished for SUJ2. In most cases, two small holes, diameter = depth = 200 µm in SUY1; 100 µm in SUJ2, were drilled onto the specimen surfaces at different spacings, *s*, varying as $0.5d_2$, d_2 or $1.5d_2$, as shown in Fig. 4(a). In order to investigate the effect of stress gradient near the notch tip, sharp notches, having the same $\sqrt{area}$ as the drilled hole, were also introduced onto the surface of SUJ2

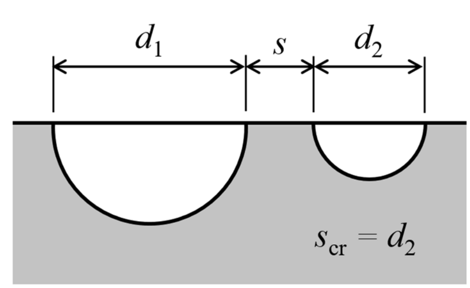

Fig. 1. The definition of the analytically-derived critical distance in interaction [1,32,34].

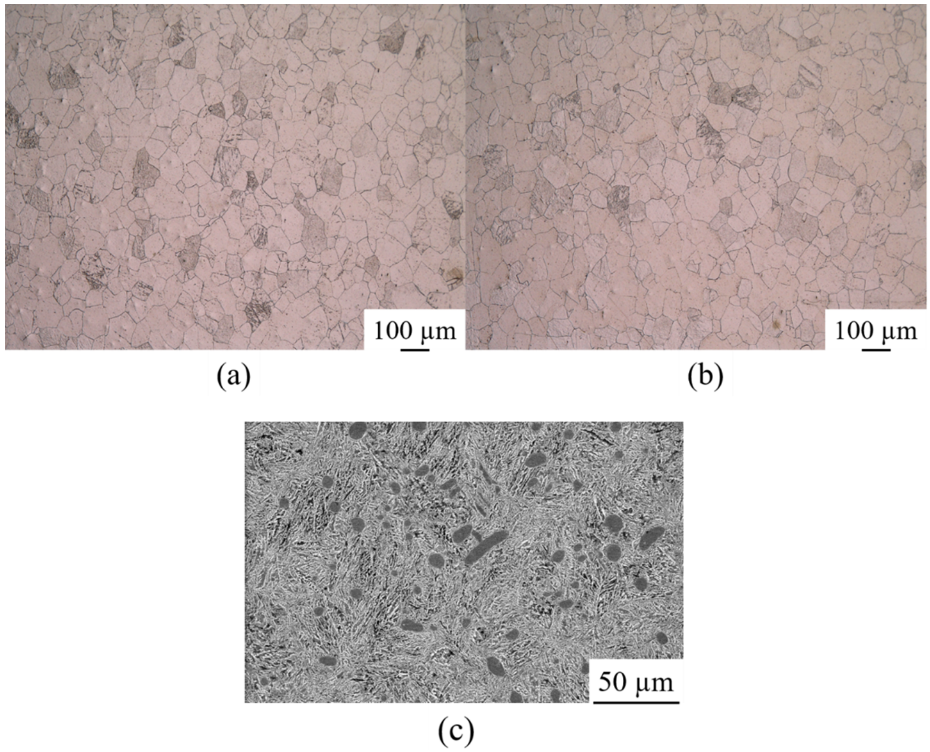

Fig. 2. The microstructure of (a) JIS-SUY1 before annealing, (b) JIS-SUY1 after annealing and (c) JIS-SUJ2.

Table 1
Mechanical properties of SUY1 and SUJ2. $\sigma_{0.2}$ is 0.2% proof stress, σ_y is yield stress, σ_b is tensile strength and *HV* is Vickers hardness.

Material	$\sigma_{0.2}$ or σ_y (MPa)	σ_b (MPa)	Reduction of area (%)	*HV*
NA-SUY1	350	420	unknown	165
A-SUY1	260	313	71	110
SUJ2	2131	2323	3	710

Table 2
Chemical compositions of SUY1 and SUJ2 (mass-%).

SUY1	C	Si	Mn	P	S	Cu	Ni	Cr
	0.004	< 0.01	0.25	0.01	0.004	0.01	0.02	0.02
SUJ2	C	Si	Mn	Cr	Ti	O		
	1.00	0.26	0.36	1.44	0.002	0.0006		

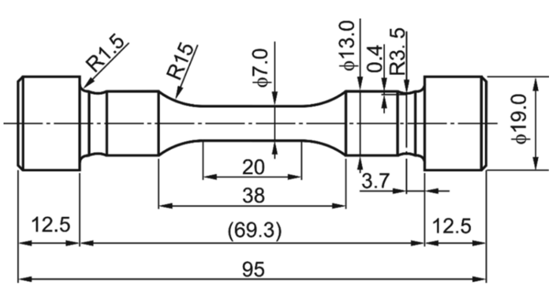

Fig. 3. Shape and dimensions of the fatigue specimen (in mm).

specimens, as revealed in Fig. 4(b). Sharp notches were made by Electric Discharge Machining (EDM) method. The notch root radius, ρ, of EDM notches ranges from 3.6 to 4.0 μm, whereas the ρ of drilled holes is half of the diameter.

2.3. Fatigue testing

Fatigue tests were performed using servo-hydraulic testing machines under fully-reversed, tension–compression loading (stress ratio, $R = -1$), at test frequencies of 10–20 Hz. Fatigue limits were determined by testing at stress steps of 10–20 MPa. Each fatigue limit was defined as the maximum stress amplitude at which a specimen ceased to fail after 10^7 cycles. Each specimen was used only once at the constant stress amplitude. The fatigue limit was predicted using the $\sqrt{area}$ parameter model referenced in Eq.1 [47]. The effective $\sqrt{area}$ was established based on the analytical critical distance criteria, as explained in the previous section.

3. Results

3.1. Fatigue test results

Fig. 5 shows the *S-N* diagrams, while all results are summarized in Table 3. Regarding the NA-SUY1 samples, the fatigue limit at the analytical critical distance ($s = d_2$) was the same as that of a single defect (160 MPa). When $s = 0.5d_2$, the fatigue limit decreased to 140 MPa, due to crack coalescence. Moreover, when $s = 1.5d_2$, the fatigue limit was marginally lower than that of a single defect (150 MPa). This is most probably due to a normal scatter, which typically results from differences in local microstructure. Similar scatter can be observed also in other materials, see *e.g.* [46]. The local microstructure causes scatter not only in the fatigue limit but also in the fatigue life. For example, in Fig. 5 (a), the life of a single hole specimen is shorter than that of a specimen with two holes under the same loading condition. On the other hand, the fatigue limit of A-SUY1 was 140 MPa regardless of the spacing between the defects, see Fig. 5 (b). The fatigue limit of SUJ2 was greatly dependent on the shape of the particular defect, see Fig. 5 (c). With regard to the drilled holes, the fatigue limit was 500 MPa, whereas in the presence of sharp notches, the fatigue limit was only 380 MPa ($s = 0.5d_2$ in both cases). It should be noted that the fatigue limit of SUJ2 was determined to be the crack

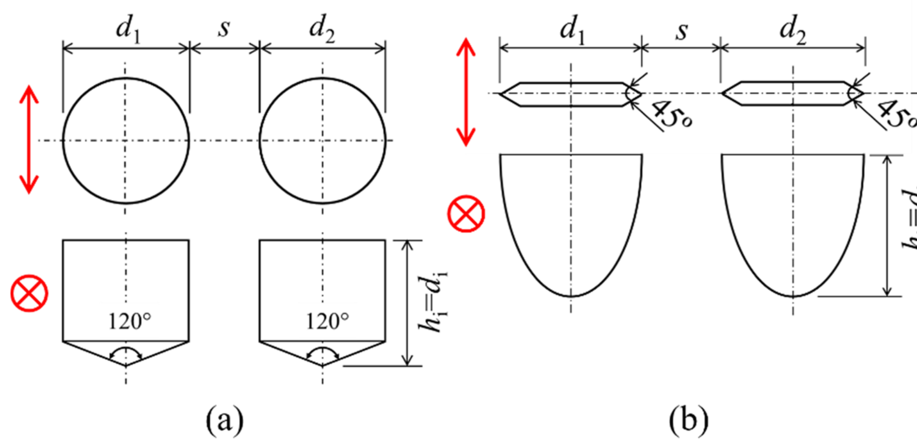

Fig. 4. Configuration of artificial defects: (a) drilled holes and (b) sharp notches. Axial directions are indicated by red marks. (For interpretation of the references to colour in this figure legend, the reader is referred to the web version of this article.)

initiation limit, controlled by the stress concentration of the defect.

3.2. Non-propagating cracks at fatigue limits

The final state of defects interacting at the fatigue limits varied radically, depending on the materials in question. In the case of SUY1, despite heat treatment, the non-propagation of cracks was evident at the fatigue limit, as illustrated in Fig. 6 (a-f). In order to observe the shape of non-propagating cracks, the specimens were broken by impact loading at −196 °C, at which the steel breaks in a brittle manner because of low-temperature embrittlement. Unfortunately, some of them were broken from other location than the non-propagating crack plane and therefore the shapes of those non-propagating cracks are not shown.

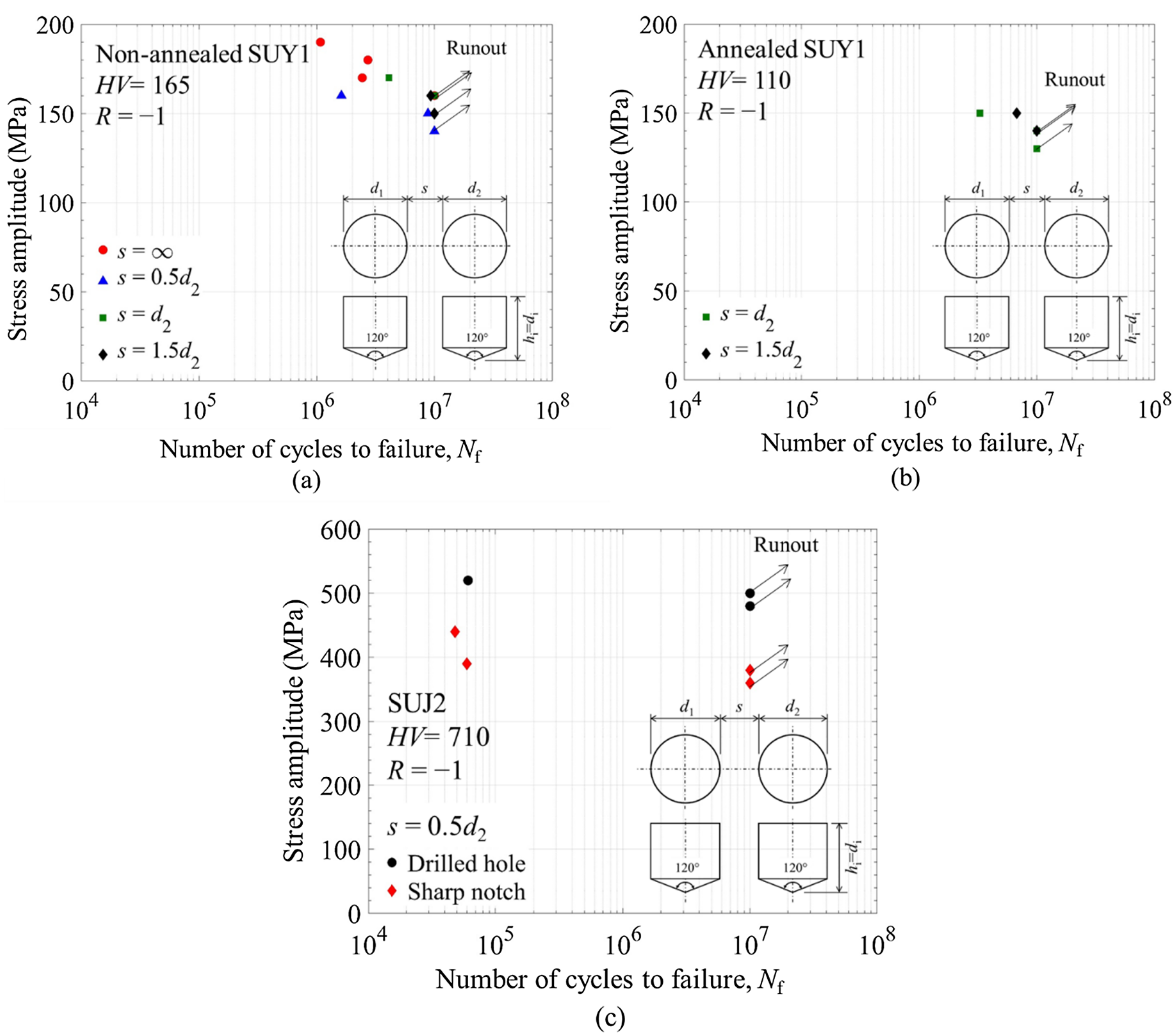

Fig. 5. *S-N* data for (a) non-annealed SUY1, (b) annealed SUY1 and (c) SUJ2.

Table 3
Summarized results of this research and results from [46]. Notations are shown in Fig. 4.

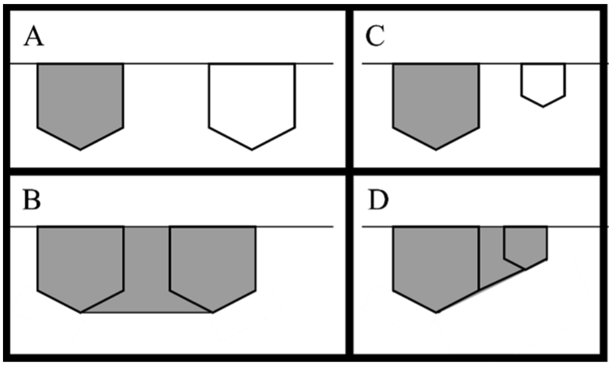

Material	Defect type (Fig. 4)	(d_1, d_2, s) [μm] (Fig. 4) $d_i = h_i$	Schematic $area_{eff}$	√*area* [μm]	$\sigma_{w,\ pred}$ [MPa]	$\sigma_{w,\ exp}$ [MPa]
Annealed SUY1	Drilled hole	(200, 200, 200)	A	177	139	140
(HV = 110)	Drilled hole	(200, 200, 300)	A	177	139	140
Non-annealed SUY1	Drilled hole	(200, -, -)	A	177	172	160
(HV = 165)	Drilled hole	(200, 200, 100)	B	350	153	140
	Drilled hole	(200, 200, 200)	A	177	172	160
	Drilled hole	(200, 200, 300)	A	177	172	150
S45C	Drilled hole	(100, -, -)	A	89	206	180
(HV = 186)	Drilled hole	(100, 100, 50)	B	140	192	175
	Drilled hole	(100, 100, 100)	A	89	206	180
	Drilled hole	(100, 100, 150)	A	89	206	190
	Drilled hole	(200, 100, 50)	D	223	177	170
	Drilled hole	(200, 100, 100)	C	177	184	170
	Drilled hole	(200, 100, 150)	C	177	184	170
SUJ2	Drilled hole	(100, 100, 50)	B	140	562	500
(HV = 710)	Sharp notch	(100, 100, 50)	B	140	562	380

The non-propagating cracks in A-SUY1 ($HV = 110$) were approximately 1-mm-long and artificial defects coalesced despite the spacing ($s = d_2$ or $1.5d_2$). Furthermore, with respect to A-SUY1, the fatigue limit was the same (140 MPa) regardless of the spacing between defects. Experiments with smaller spacings were not considered relevant, since the interaction was already confirmed to occur at the critical distance $s = d_2$ and even when $s = 1.5d_2$.

Regarding NA-SUY1 ($HV = 165$), the defects behaved as individual cracks without coalescence at the fatigue limit when the spacing between defects was greater than the critical distance, *i.e.,* when $s > d_2$, whereas at $s \leq d_2$, the defects behaved together as a single larger crack, with non-propagating cracks coalescing at the fatigue limit. It is noteworthy that cracks emanating from NA-SUY1 ($HV = 165$) grew transgranularly, while in A-SUY1 ($HV = 110$), the cracks essentially grew along grain boundaries, see Fig. 6.

In contrast, in the context of bearing steel SUJ2 ($HV = 710$), no non-propagating cracks were observed at the fatigue limit in all cases, see Fig. 6 (g-h). Therefore, the crack initiation limit was also considered to be the fatigue limit. Interaction did not occur even at $s = 0.5d_2$, implying that the real critical distance for SUJ2 is considerably smaller. The authors therefore elected not to investigate larger spacings.

4. Discussion

4.1. Comparison of the predicted and experimental fatigue limits

Fig. 7 shows the fatigue limits normalized by prediction values. It is clearly demonstrated that the $\sqrt{area}$ parameter model [47] can accurately predict fatigue limits, even in the framework of interaction problems. Throughout this research, the effective prediction area was determined according to an assumption of the analytical critical distance in all cases. Fig. 7 shows that the $\sqrt{area}$ parameter model can apparently also predict the SUJ2 drilled-hole fatigue limit, that is, the crack initiation limit. However, since the $\sqrt{area}$ parameter model is based on fracture mechanics, it may be just pure coincidence that it can also predict the crack-initiation limit of a drilled hole. In reality, since a drilled hole behaved precisely like a blunt notch in SUJ2, it would therefore have been more appropriate to use some of the well-established, fatigue-notch methods. The SUJ2 results are discussed in further detail later in this section.

To investigate the minimum size of the detrimental defect in SUY1, which behaves as a fracture origin instead of the persistent slip bands in large grains, grain sizes were inspected based on the statistics of extremes [49] in a manner similar to that recorded in the literature [1]. Grain size analysis was undertaken for NA-SUY1. It was not repeated for A-SUY1 since grain size was not influenced by annealing, see Fig. 2(a) and (b). The results of the grain size analysis are documented in Fig. 8. As shown in Fig. 2, the average grain size of SUY1 was approximately 60 μm, while the largest grain size was approximately 200 μm, according to Fig. 8. The result inferred that a defect smaller than 200 μm would not be expected to become a fracture origin. Under fatigue loading, the fracture origin in low- and moderate-strength materials is typically the largest grain on the surface. The persistent slip bands create cumulative dislocations within a grain, eventually penetrate the entire grain and become a crack [1]. Therefore, larger grains would naturally result in larger naturally occurring cracks and defects smaller than the largest grain would not become fracture origins [1]. Consequently, drilled holes of 200 μm were employed during the SUY1 experiments. It is noteworthy to mention that the absolute size of defects does not influence the analytical interaction criteria, since the interaction (or not) of cracks is determined by the ratio, s/d_2, (*i.e.,* if $s/d_2 > 1$, the interaction effect is negligible).

4.2. The influence of non-propagating crack size on crack coalescence and fatigue limit

The material-independent analytical models are based on variations in elastic stress distributions and an increase in stress intensity factors due to the existence of neighboring defects. In view of the experimental findings presented in this study, it is clear that the analytical interaction criteria must be considered with caution in practical applications. This is because the behavior of interacting small defects at the fatigue limit varies between materials due to differences in the characteristics of non-propagating cracks. For example, it has been suggested that defect orientation [12], stress ratio [11,50] and dual-phase microstructure [46] can influence the size and location of non-propagating cracks. However, notwithstanding other factors, a non-propagating crack usually tends to appear as a result of plasticity-induced crack-closure [51]. Thus, HV, which reflects materials resistance to plastic deformation, can be one of the most relevant material properties in the description of non-propagating crack characteristics. To illustrate this phenomenon, several data from literature [12,46,52–60] have been plotted in Fig. 9. All data were tested at $R = -1$. The data featured in Fig. 9 are reproduced in Table A1 in Appendix A. Fig. 9 reveals that the size of a non-propagating crack tends to diminish with an increase in hardness, although a large scatter exists. Moreover, it is evident that a non-propagating crack can hardly exist when $HV > 400$. During the course of this study, non-propagating cracks were also not observed at the fatigue limit in SUJ2 ($HV = 710$). Since experimental data are limited and not every material can be tested individually, it is very difficult to provide the exact values of HV and/or non-propagating crack size for which certain interaction criteria are always applicable. This greatly complicates the defect interaction problem. However,

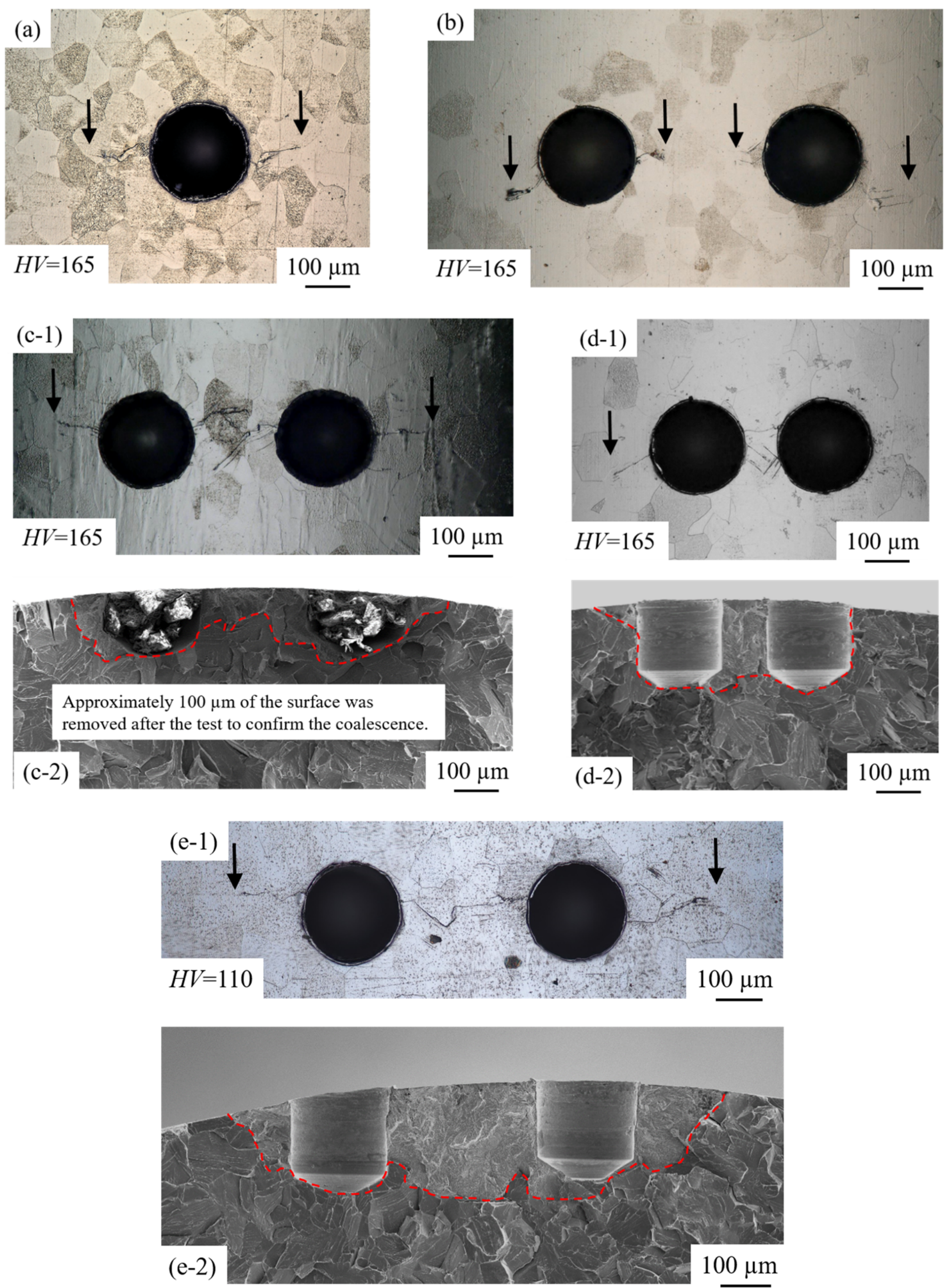

Fig. 6. Non-propagating cracks: (a) NA-SUY1, single defect; (b) NA-SUY1, $s = 1.5d_2$; (c) NA-SUY1, $s = d_2$; (d) NA- SUY1, $s = 0.5d_2$; (e) A-SUY1, $s = 1.5d_2$; (f) A-SUY1, $s = d_2$; (g) SUJ2, $s = 0.5d_2$, drilled holes; (h) SUJ2, $s = 0.5d_2$, sharp notches. The surfaces of SUJ2 specimens were electro-polished after the tests to confirm the absence of cracks.

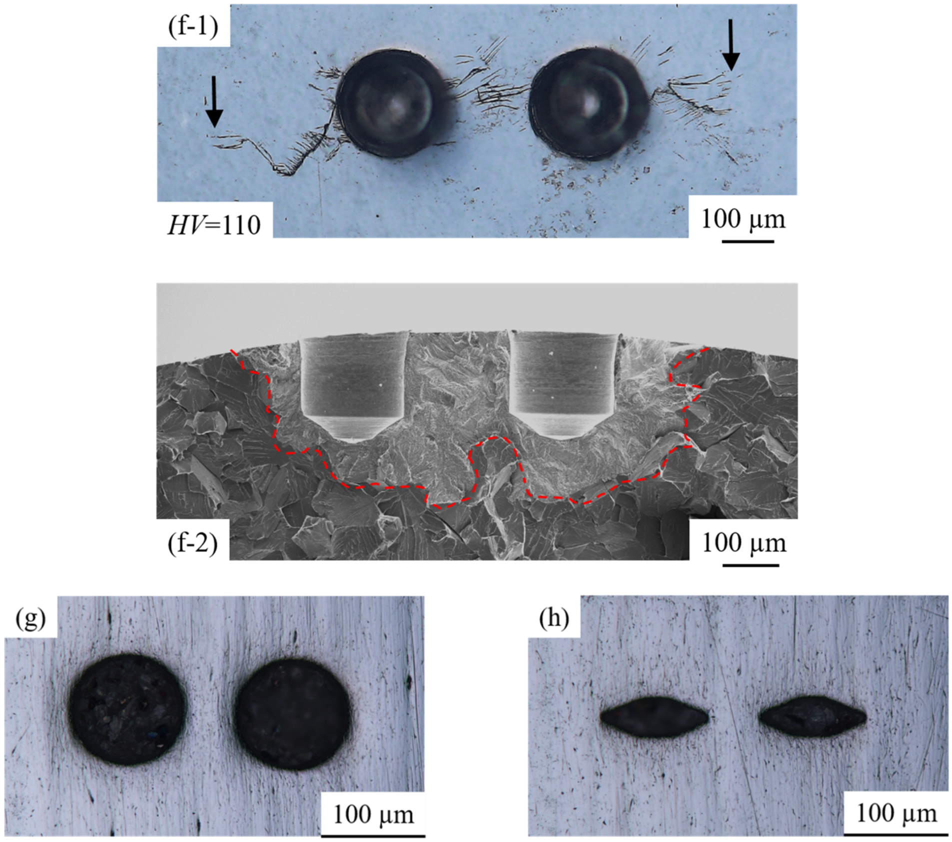

Fig. 6. (*continued*)

regarding the current experimental results presented herein and in the previous by Åman *et al.* [46], it is possible to consider the extreme cases of very low and very high *HV*, as well as intermediate *HV* cases separately.

4.3. The interaction effect in soft steels

For instance, in the context of the softest material tested, A-SUY1 ($HV = 110$), the non-propagating cracks are of particular interest, on display in Fig. 6 (e) and (f). The total length of coalesced non-propagating cracks, regardless of the spacing between defects, was approximately 1 mm, *i.e.,* five times larger than the initial defect size. According to analytical interaction criteria, the defects should be acknowledged to be individual if the spacing between them is larger than the diameter of the smaller defect, *i.e.,* when $s > d_2$. Since the defects definitely behaved in the manner of a larger single defect, even when $s = 1.5d_2$, the analytical interaction criteria apparently does not apply to materials with non-propagating cracks as long as those observed for A-SUY1. It is interesting to note that the fatigue limit was the same (140 MPa) regardless of the spacing between defects and despite crack coalescence. Nevertheless, if the spacing between defects were to increase beyond a certain value, crack coalescence might begin to

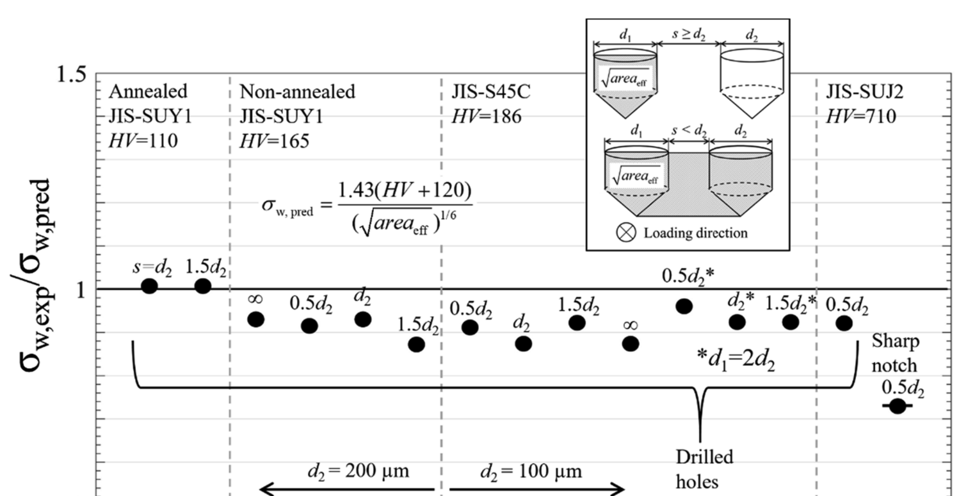

Fig. 7. Comparison of the predicted and experimental fatigue limits. S45C data have been reproduced [46].

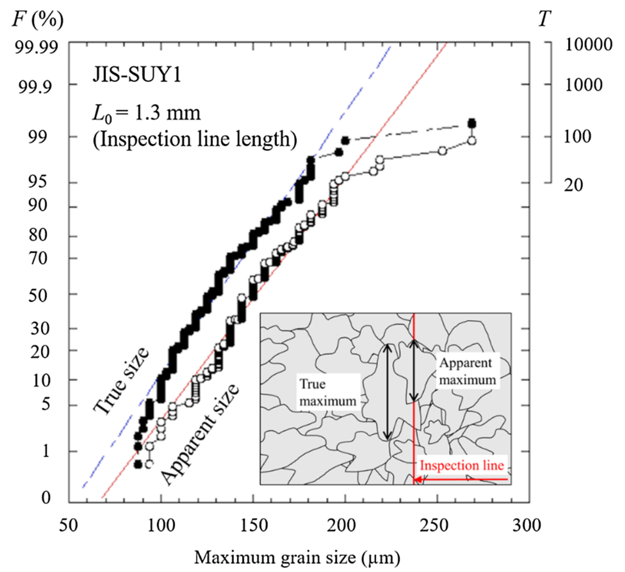

Fig. 8. Grain size analysis of non-annealed SUY1 based on statistics of extremes.

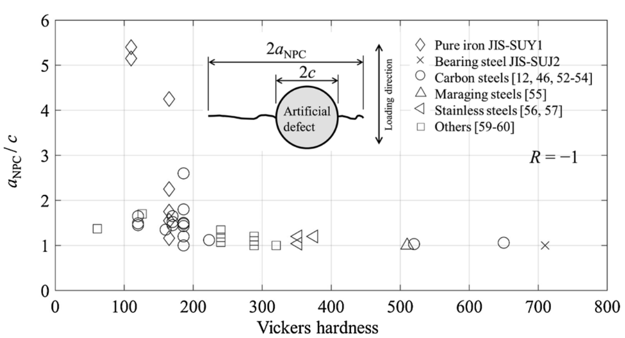

Fig. 9. Relative size of non-propagating crack as a function of *HV*. [12,46,52–60].

decrease the fatigue limit, as the newly-formed coalesced crack may exceed the material's crack-propagation threshold simply due to its size. From a fatigue limit viewpoint, this implies that the real critical distance of such a material is in fact longer than the analytical one.

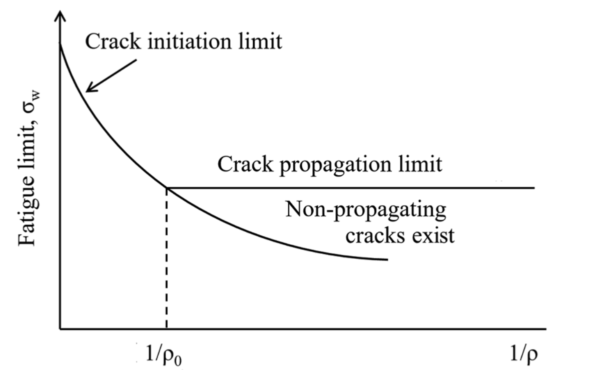

Fig. 11. Crack initiation and propagation limits versus the inverse of notch root radius [67].

4.4. The interaction effect in hard steels

On the contrary, in the high-strength bearing steel SUJ2 ($HV = 710$), unlike in every other material tested, the interacting defects behaved clearly as individual defects, even when the spacing between them was smaller than the analytical critical distance. No defect interaction was observed for $s = 0.5d_2$, which is significantly smaller than the proposed analytical critical distance, $s = d_2$. If the spacing between the defects would have been further decreased, it could be expected that the stress in the region between the defects would reach the crack initiation limit and defects would have coalesced. As referenced in Fig. 9, since non-propagating cracks can hardly exist when $HV > 400$, the fatigue limit of such higher-strength steels is determined more or less by crack initiation. Consequently, the real critical distance for high-strength steels correlates with the crack-initiation threshold.

4.4.1. Small crack or large crack?

The evaluation of fatigue crack growth and its threshold via linear elastic fracture mechanics (LEFM) postulates that the small scale yielding condition holds. This requires that the plastic zone size is sufficiently small compared to the crack size and remains constant under a constant stress intensity. In such a regime, ΔK_{th} becomes independent of crack size. On the other hand, when the defect is small and applied stress level is high, the plastic zone is no longer small compared to the crack size. In such a regime, the crack-tip yielding satisfies the large scale yielding condition, where ΔK_{th} is decreased with

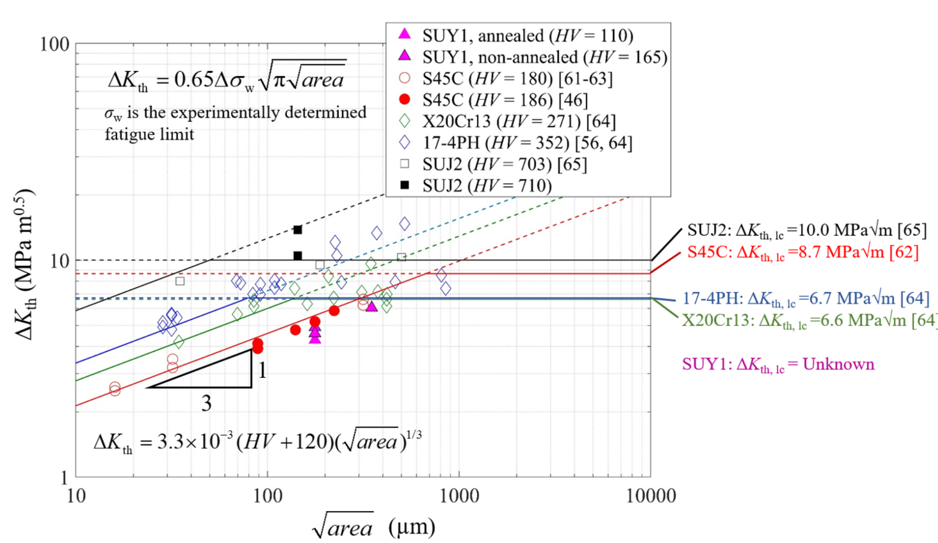

Fig. 10. ΔK_{th} for various materials. $\Delta K_{th,\ lc}$ is associated with long cracks [46,56,61–65].

a decrease in crack size. The $\sqrt{area}$ parameter model targets the latter case. Namely, this model is applicable to the small crack, but not to the large crack.

As exhibited in Fig. 7, the fatigue limit of the SUJ2 having drilled hole was in good agreement with the prediction by the $\sqrt{area}$ parameter model (*i.e.*, $\sigma_{w,exp}/\sigma_{w,pred} = 0.89$). On the contrary, the fatigue limit of sharp-notched SUJ2 was well below the predicted value (*i.e.*, $\sigma_{w,exp}/\sigma_{w,pred} = 0.68$). This phenomenon can be understood as follows. Fig. 10 depicts the ΔK_{th} for various materials as a function of the defect/crack size [46,56,61–65]. As pointed out by Chapetti [66], the small/large crack-transition size is more or less dependent on *HV, i.e.,* the higher the *HV*, the smaller the transition size. According to Fig. 10, the transition point of $\sqrt{area}$ is approximately 50 µm for SUJ2, which is smaller than the size of the defects used in the present tests. Therefore, the $\sqrt{area}$ parameter model overestimates the crack growth threshold in the large crack regime (dashed lines in Fig. 10). In addition, in the present experiments, the fatigue limits of the drill-holed and sharp-notched specimens were both determined from crack initiation that is controlled by the stress concentration of the defect. As a result, the fatigue limit of a drill-holed specimen is higher than that of a sharp-notched specimen.

4.4.2. Crack or notch?

As expounded by Nisitani [67] and shown in Fig. 11, the critical notch-root radius, ρ_0, is a material-dependent parameter that determines whether a defect behaves like a blunt notch or as a crack. If the notch root radius ρ is smaller than ρ_0, two fatigue limits, one for crack initiation and the other for crack propagation, can be distinguished. In a variety of materials, the ρ_0 typically measures about 0.4–0.5 mm, but can decrease to less than 0.1 mm as tensile strength increases [67]. The experimental results infer that the ρ_0 of SUJ2 ($\sigma_{0.2}$ = 2131 MPa) is likely to be so small that the crack initiation and propagation limits were not possible to distinguish and that the fatigue limit was determined from crack initiation. The values of ρ_0 may also vary depending on the notch size for small defects, *i.e.,* length or depth of the notch [67]. In fact, Schönbauer [64] performed ultrasonic fatigue tests of stainless steels (UTS = 878–1030 MPa) and established the ρ_0 to be less than 25 µm. The authors are not aware of any method to reliably predict ρ_0 other than experimentally, especially for the defects smaller than 1 mm. In cases where the notch root radius in a component is larger than ρ_0, notch-based methods to assess fatigue strength are preferred rather than fracture mechanics-based approach. However, in reality, as was pointed out by Murakami [1], the defects generally include locally higher stress concentrations and therefore fracture mechanics-based evaluation can provide a reasonable prediction in many instances.

4.5. The interaction effect in moderate strength steels

In the moderate-strength steels NA-SUY1 (*HV* = 165) and S45C (*HV* = 186) [46], the analytical critical distance criteria seem to hold well when compared with the two afore-mentioned extreme cases. Yet, the dual-phase microstructure especially tends to exhibit larger scatter in non-propagating crack size and location(s), leading to larger scatter in fatigue limit [46]. For a material with such a complex microstructure, the selection of conservative criteria is recommended, *i.e.,* the interaction should be assumed to occur even when $s = d_2$.

4.6. Future works

In the authors' previous work [46], it was revealed that if $d_1 = 2d_2$, only the larger defect would control the fatigue limit, regardless of the existence of the smaller defect and of the spacing between the defects. For this reason, two defects of identical size were employed in this study. Notwithstanding, it is yet unclear whether this applies to any material and what actually are the boundary conditions for the size effect in interaction. Another interesting future work would be to determine the threshold condition for crack initiation and to estimate the real critical distance in materials exhibiting non-propagating cracks larger than the initial defect size. In addition, the interaction effect under diverse loading conditions is of interest, as well as the interaction study considering problems including different defect shapes, orientations and location configurations.

5. Conclusions

The two defects were introduced onto the surface of pure iron SUY1 and bearing steel SUJ2 specimens in order to investigate the fatigue limit interaction effect and its material dependency. The experimental results complemented those previously obtained on the medium carbon steel JIS-S45C. The summarized results underlined the fact that the analytical interaction criteria are insufficient for identifying the interaction effect in all materials. The analytical models are based on the variations in elastic stress distributions due to the existence of neighboring defects, neglecting the features of non-propagating cracks. The following conclusions were drawn from the experimental findings:

- Defects coalesced at the fatigue limit in annealed JIS-SUY1 (*HV* = 110), regardless of the spacing between them. Non-propagating cracks were approximately five times larger than the initial defect size. The fatigue limit and non-propagating crack sizes were independent of the spacing between the defects.
- Since no non-propagating cracks were observed in JIS-SUJ2, the fatigue limit was determined from crack initiation. Neither defect type, drilled holes nor sharp notches, interacted at the fatigue limit even when the spacing between the defects was less than the analytical critical distance.
- The analytical critical distance applies only for moderate *HV* materials. In reality, it appears that the critical distance is smaller than the analytical one in high-strength steels (*HV* > 400) and *vice versa,* when low-strength steels are concerned.
- Murakami's $\sqrt{area}$ parameter model also accurately predicted the fatigue limits of interacting small defects. The only exception involved the bearing steel SUJ2, the fatigue limit of which was identified as the crack initiation limit. Thus, the fracture mechanics-based $\sqrt{area}$ parameter model was not applicable.
- The characteristics of non-propagating cracks significantly affect crack coalescence and consequently, the behavior of interacting cracks, thereby rendering the interaction phenomena complicated. Non-propagating crack size tends to decrease with the increased hardness of a material, although there is a large scatter.

Declaration of Competing Interest

The authors declare that they have no known competing financial interests or personal relationships that could have appeared to influence the work reported in this paper.

Acknowledgements

The present research was financially supported by Aalto University, School of Engineering and by the Academy of Finland (decisions no. 298762). The financial support is gratefully appreciated.

Appendix A

See Fig. A1 and Table A1.

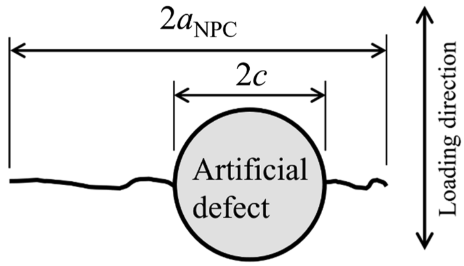

Fig. A1. Notations for Table A1.

Table A1
Data used for Fig. 9. T-C = tension–compression, R-B = rotating-bending.

HV	$\sqrt{area_{eff}}$	2*c* (μm)	$2a_{NPC}$ (μm)	a_{NPC}/c	Defect type	Material	Testing method	Reference
186	89	100	100	1.00	Drilled hole	JIS-S45C	T-C servo-hydraulic	[46]
186	140	250	370	1.48	Drilled hole	JIS-S45C	T-C servo-hydraulic	[46]
186	140	250	300	1.20	Drilled hole	JIS-S45C	T-C servo-hydraulic	[46]
186	140	250	250	1.00	Drilled hole	JIS-S45C	T-C servo-hydraulic	[46]
186	140	250	250	1.00	Drilled hole	JIS-S45C	T-C servo-hydraulic	[46]
186	89	100	150	1.50	Drilled hole	JIS-S45C	T-C servo-hydraulic	[46]
186	89	100	100	1.00	Drilled hole	JIS-S45C	T-C servo-hydraulic	[46]
186	89	100	100	1.00	Drilled hole	JIS-S45C	T-C servo-hydraulic	[46]
186	89	100	100	1.00	Drilled hole	JIS-S45C	T-C servo-hydraulic	[46]
186	89	100	180	1.80	Drilled hole	JIS-S45C	T-C servo-hydraulic	[46]
186	223	350	500	1.43	Drilled hole	JIS-S45C	T-C servo-hydraulic	[46]
186	177	200	200	1.00	Drilled hole	JIS-S45C	T-C servo-hydraulic	[46]
186	177	100	260	2.60	Drilled hole	JIS-S45C	T-C servo-hydraulic	[46]
165	177	200	450	2.25	Drilled hole	Non-annealed JIS-SUY1	T-C servo-hydraulic	Authors
165	280	500	580	1.16	Drilled hole	Non-annealed JIS-SUY1	T-C servo-hydraulic	Authors
165	177	200	850	4.25	Drilled hole	Non-annealed JIS-SUY1	T-C servo-hydraulic	Authors
165	177	200	310	1.55	Drilled hole	Non-annealed JIS-SUY1	T-C servo-hydraulic	Authors
165	177	200	350	1.75	Drilled hole	Non-annealed JIS-SUY1	T-C servo-hydraulic	Authors
110	177	200	1030	5.15	Drilled hole	Annealed JIS-SUY1	T-C servo-hydraulic	Authors
110	177	200	1080	5.40	Drilled hole	Annealed JIS-SUY1	T-C servo-hydraulic	Authors
710	89	100	100	1.00	Drilled hole	JIS-SUJ2	T-C servo-hydraulic	Authors
710	140	250	250	1.00	Drilled hole	JIS-SUJ2	T-C servo-hydraulic	Authors
710	89	100	100	1.00	sharp notch	JIS-SUJ2	T-C servo-hydraulic	Authors
710	140	250	250	1.00	Sharp notch	JIS-SUJ2	T-C servo-hydraulic	Authors
170	35	40	58	1.45	Drilled hole	0.46-C steel	R-B	[52]
170	89	100	152	1.52	Drilled hole	0.46-C steel	R-B	[52]
170	177	200	330	1.65	Drilled hole	0.46-C steel	R-B	[52]
510	63	100	100	1.00	Drilled hole	Maraging steel	R-B	[55]
510	63	100	100	1.00	Pre-crack	Maraging steel	R-B	[55]
510	63	100	100	1.00	Pre-crack	Maraging steel	R-B	[55]
650	71	80	85	1.06	Drilled hole	Q S45C	R-B	[53]
520	133	150	155	1.03	Drilled hole	QT S45C	R-B	[53]
120	35	40	58	1.45	Drilled hole	0.13-C steel	R-B	[52]
120	89	100	149	1.49	Drilled hole	0.13-C steel	R-B	[52]
120	177	200	330	1.65	Drilled hole	0.13-C steel	R-B	[52]
240	45	59	79	1.34	Corrosion pit	12% Cr steam turbine blade steel	Ultrasonic	[58]
240	90	114	134	1.18	Corrosion pit	12% Cr steam turbine blade steel	Ultrasonic	[58]
240	232	292	312	1.07	Corrosion pit	12% Cr steam turbine blade steel	Ultrasonic	[58]
352	92	50	60	1.20	Corrosion pit	17-4PH stainless steel	Ultrasonic	[56]
352	35	50	60	1.20	Drilled hole	17-4PH stainless steel	T-C servo-hydraulic	[56]
352	35	50	52	1.04	Drilled hole	17-4PH stainless steel	T-C servo-hydraulic	[56]
117	188	300	642	2.14	Sharp notch	JIS-S15C	T-C	[12]
117	188	205	230	1.12	Drilled hole	JIS-S15C	T-C	[12]
186	188	300	497	1.66	Sharp notch	JIS-S45C	T-C	[12]
186	188	205	512	2.50	Drilled hole	JIS-S45C	T-C	[12]
126	227	400	680	1.70	Sharp notch	Fe-C (Fully-ferritic steel)	R-B	[59]
61	337	600	820	1.37	Sharp notch	IF (Interstitial-free) steel	R-B	[59]
288	925	1000	1000	1.00	Drilled hole	Ti-6Al-4V	T-C	[60]
320	453	760	760	1.00	Drilled hole	Ti-6Al-4V	T-C	[60]
320	239	400	400	1.00	Drilled hole	Ti-6Al-4V	T-C	[60]
288	185	200	200	1.00	Drilled hole	Ti-6Al-4V	T-C	[60]
288	185	200	220	1.10	Hole with burr	Ti-6Al-4V	T-C	[60]
288	46	50	60	1.20	Hole with burr	Ti-6Al-4V	T-C	[60]
375	89	100	120	1.20	Drilled hole	Fe-25Cr-1N (Stainless steel)	R-B	[57]
223	61.5	100	112	1.12	EDM notch	0.84-C steel	R-B	[54]
160	104	144	194	1.35	EDM notch	0.36-C steel	R-B	[54]

References

[1] Murakami Y. Metal fatigue: effects of small defects and nonmetallic inclusions. Academic Press; 2019.

[2] Endo M, Yanase K. Effects of small defects, matrix structures and loading conditions on the fatigue strength of ductile cast irons. Theor Appl Fract Mech 2014;69:34–43. https://doi.org/10.1016/j.tafmec.2013.12.005.

[3] Jono M, Sugeta A. Crack closure and effect of load variation on small fatigue crack growth behaviour. Fatigue Fract Eng Mater Struct 1996;19(2–3):165–74. https://doi.org/10.1111/j.1460-2695.1996.tb00956.x.

[4] Léopold G, Nadot Y, Billaudeau T, Mendez J. Influence of artificial and casting defects on fatigue strength of moulded components in Ti-6Al-4V alloy. Fatigue Fract Eng Mater Struct 2015;38(9):1026–41. https://doi.org/10.1111/ffe.12326.

[5] Matsunaga H, Shomura N, Muramoto S, Endo M. Shear mode threshold for a small fatigue crack in a bearing steel. Fatigue Fract Eng Mater Struct 2011;34(1):72–82. https://doi.org/10.1111/j.1460-2695.2010.01495.x.

[6] Socie DF, Hua CT, Worthem DW. Mixed mode small crack growth. Fatigue Fract Eng Mater Struct 1987;10(1):1–16.

[7] Morel F, Guerchais R, Saintier N. Competition between microstructure and defect in multiaxial high cycle fatigue. Frattura ed Integrità Strutturale 2015;33:404–14. https://doi.org/10.3221/IGF-ESIS.33.45.

[8] Tokaji K, Ogawa T, Aoki T. Small fatigue crack growth in a low carbon steel under tension–compression and pulsating-tension loading. Fatigue Fract Eng Mater Struct 1990;13(1):31–9. https://doi.org/10.1111/j.1460-2695.1990.tb00574.x.

[9] Nishimura Y, Yanase K, Ikeda Y, Tanaka Y, Miyamoto N, Miyakawa S, et al. Fatigue strength of spring steel with small scratches. Fatigue Fract Eng Mater Struct 2018;41(7):1514–28. https://doi.org/10.1111/ffe.12793.

[10] Kashiwagi M, Kudou T, Kubota M, Sakae C, Kondo Y. Effect of crack closure on the fatigue limit of material containing small defect. Zairyo/J Soc Mater Sci, Jpn 2003;52(11):1345–50. https://doi.org/10.2472/jsms.52.1345.

[11] Kondo Y, Sakae C, Kubota M, Kudou T. The effect of material hardness and mean stress on the fatigue limit of steels containing small defects. Fatigue Fract Eng Mater Struct 2003;26(8):675–82. https://doi.org/10.1046/j.1460-2695.2003.00656.x.

[12] Lorenzino P, Okazaki S, Matsunaga H, Murakami Y. Effect of small defect orientation on fatigue limit of carbon steels. Fatigue Fract Eng Mater Struct 2015;38(9):1076–86. https://doi.org/10.1111/ffe.12321.

[13] Zerbst U, Madia M. Fracture mechanics based assessment of the fatigue strength: approach for the determination of the initial crack size. Fatigue Fract Eng Mater Struct 2015;38(9):1066–75. https://doi.org/10.1111/ffe.12288.

[14] Serrano-Munoz I, Buffiere JY, Verdu C, Gaillard Y, Mu P, Nadot Y. Influence of surface and internal casting defects on the fatigue behaviour of A357–T6 cast aluminium alloy. Int J Fatigue 2016;82:361–70. https://doi.org/10.1016/j.ijfatigue.2015.07.032.

[15] Hrabe N, Gnäupel-Herold T, Quinn T. Fatigue properties of a titanium alloy (Ti–6Al–4V) fabricated via electron beam melting (EBM): Effects of internal defects and residual stress. Int J Fatigue 2017;94:202–10. https://doi.org/10.1016/j.ijfatigue.2016.04.022.

[16] Madia M, Schork B, Bernhard J, Kaffenberger M. Multiple crack initiation and propagation in weldments under fatigue loading. Procedia Struct Integrity 2017;7:423–30. https://doi.org/10.1016/j.prostr.2017.11.108.

[17] Otegui JL, Kerr HW, Burns DJ, Mohaupt UH. Fatigue crack initiation from defects at weld toes in steel. Int J Press Vessels Pip 1989;38(5):385–417. https://doi.org/10.1016/0308-0161(89)90048-3.

[18] Leitner M, Murakami Y, Farajian M, Remes H, Stoschka M. Fatigue Strength Assessment of Welded Mild Steel Joints Containing Bulk Imperfections. Metals 2018;8(5):306. https://doi.org/10.3390/met8050306.

[19] Takahashi K, Murakami Y. Quantitative evaluation of effect of surface roughness on fatigue strength. Eng Against Fatigue 1999:693–703.

[20] Murakami Y, Tsutsumi K, Fujishima M. Quantitative evaluation of effect of surface roughness on fatigue strength. Trans Jpn SOC Mech Eng Ser A 1996;63597:1124–31.

[21] Kawamoto M, Nishioka K, Inui T, Tsuchiya F. The influence of surface roughness of specimens on fatigue strength under rotating-beam test. J Soc Mater Sci Jpn 1955;4:42–8.

[22] Murakami Y, Kodama S, Konuma S. Quantitative evaluation of effects of non-metallic inclusions on fatigue strength of high strength steels. I: Basic fatigue mechanism and evaluation of correlation between the fatigue fracture stress and the size and location of non-metallic inclusions. Int J Fatigue 1989;11(5):291–8. https://doi.org/10.1016/0142-1123(89)90054-6.

[23] Karr U, Schuller R, Fitzka M, Schönbauer B, Tran D, Pennings B, et al. Influence of inclusion type on the very high cycle fatigue properties of 18Ni maraging steel. J Mater Sci 2017;52(10):5954–67.

[24] Matsunaga H, Sun C, Hong Y, Murakami Y. Dominant factors for very-high-cycle fatigue of high-strength steels and a new design method for components. Fatigue Fract Eng Mater Struct 2015;38(11):1274–84. https://doi.org/10.1111/ffe.12331.

[25] Yamashita Y, Murakami T, Mihara R, Okada M, Murakami Y. Defect analysis and fatigue design basis for Ni-based superalloy 718 manufactured by selective laser melting. Int J Fatigue 2018;117:485–95. https://doi.org/10.1016/j.ijfatigue.2018.08.002.

[26] Gao W, Zhang Y, Ramanujan D, Ramani K, Chen Y, Williams CB, et al. The status, challenges, and future of additive manufacturing in engineering. Comput Aided Des 2015;69:65–89. https://doi.org/10.1016/j.cad.2015.04.001.

[27] Molaei R, Fatemi A. Fatigue design with additive manufactured metals: issues to consider and perspective for future research. Procedia Eng 2018;213:5–16. https://doi.org/10.1016/j.proeng.2018.02.002.

[28] Spierings AB, Starr TL, Wegener K. Fatigue performance of additive manufactured metallic parts. Rapid Prototyping J 2013;19(2):88–94. https://doi.org/10.1108/13552541311302932.

[29] Beretta S, Romano S. A comparison of fatigue strength sensitivity to defects for materials manufactured by AM or traditional processes. Int J Fatigue 2017;94:178–91. https://doi.org/10.1016/j.ijfatigue.2016.06.020.

[30] Masuo H, Tanaka Y, Morokoshi S, Yagura H, Uchida T, Yamamoto Y, et al. Influence of defects, surface roughness and HIP on the fatigue strength of Ti-6Al-4V manufactured by additive manufacturing. Int J Fatigue 2018;117:163–79. https://doi.org/10.1016/j.ijfatigue.2018.07.020.

[31] Murakami Y, Nemat-Nasser S. Interacting dissimilar semi-elliptical surface flaws under tension and bending. Eng Fract Mech 1982;16(3):373–86. https://doi.org/10.1016/0013-7944(82)90115-1.

[32] Murakami Y, Nemat-Nasser S. Growth and stability of interacting surface flaws of arbitrary shape. Eng Fract Mech 1983;17(3):193–210. https://doi.org/10.1016/0013-7944(83)90027-9.

[33] Nisitani H, Murakami Y. Stress intensity factors for interacting equal semi-elliptical surface cracks in tension. Trans Jpn Soc Mech Eng JSME 1981;47:295–303.

[34] Åman M. Interacting three-dimensional surface cracks under tensile loading, Master's Thesis; 2015. Available: https://aaltodoc.aalto.fi/handle/123456789/16692 [last accessed date 11 November 2019].

[35] Noda NA, Kobayashi K, Oohashi T. Variation of the stress intensity factor along the crack front of interacting semi-elliptical surface cracks. Arch Appl Mech 2001;71(1):43–52. https://doi.org/10.1007/s004190000113.

[36] Patel SK, Dattaguru B, Ramachandra K. Multiple interacting and coalescing semi-elliptical surface cracks in fatigue-Part-I: finite element analysis. Struct Longevity 2010;3(1–2):37–57.

[37] Newman JC, Jr., Raju IS. Analyses of surface cracks in finite plates under tension or bending loads. NASA TP1578; 1979.

[38] Zhu SP, Hao YZ, Liao D. Probabilistic modeling and simulation of multiple surface crack propagation and coalescence. Appl Math Model 2020;78:383–98. https://doi.org/10.1016/j.apm.2019.09.045.

[39] Li P, Lee PD, Maijer DM, Lindley TC. Quantification of the interaction within defect populations on fatigue behavior in an aluminum alloy. Acta Mater 2009;57(12):3539–48. https://doi.org/10.1016/j.actamat.2009.04.008.

[40] Sonsino CM, Ziese J. Fatigue strength and applications of cast aluminium alloys with different degrees of porosity. Int J Fatigue 1993;15(2):75–84. https://doi.org/10.1016/0142-1123(93)90001-7.

[41] Chen Y, Zhang H, Zhang J, Liu X, Li X, Zhou J. Failure assessment of X80 pipeline with interacting corrosion defects. Eng Fail Anal 2015;47:67–76. https://doi.org/10.1016/j.engfailanal.2014.09.013.

[42] Silva RCC, Guerreiro JNC, Loula AFD. A study of pipe interacting corrosion defects using the FEM and neural networks. Adv Eng Softw 2007;38(11–12):868–75. https://doi.org/10.1016/j.advengsoft.2006.08.047.

[43] Al-Owaisi S, Becker AA, Sun W, Al-Shabibi A, Al-Maharbi M, Pervez T, et al. An experimental investigation of the effect of defect shape and orientation on the burst pressure of pressurised pipes. Eng Fail Anal 2018;93:200–13. https://doi.org/10.1016/j.engfailanal.2018.06.011.

[44] Galatolo R, Lazzeri R. Fatigue crack growth of multiple interacting cracks: Analytical models and experimental validation. Fatigue Fract Eng Mater Struct 2018;41(1):183–96. https://doi.org/10.1111/ffe.12671.

[45] Deguchi T, Matsuo T, Kim H, Ikeda T, Endo M. Fatigue strength evaluation of ferritic-pearlitic ductile cast iron with notches and holes of various sizes. Adv Exper Mech 2017;2:87–91. https://doi.org/10.11395/aem.2.0_87.

[46] Åman M, Okazaki S, Matsunaga H, Marquis GB, Remes H. Interaction effect of adjacent small defects on the fatigue limit of a medium carbon steel. Fatigue Fract Eng Mater Struct 2017;40(1):130–44. https://doi.org/10.1111/ffe.12482.

[47] Murakami Y, Endo M. Quantitative evaluation of fatigue strength of metals containing various small defects or cracks. Eng Fract Mech 1983;17(1):1–15. https://doi.org/10.1016/0013-7944(83)90018-8.

[48] Standard B. BS 7910: 2013 + A1: 2015 Guide to methods for assessing the acceptability of flaws in metallic structures. London, UK: BSI Stand Publ; 2015.

[49] Gumbel EJ. Statistics of Extremes. Courier Corporation; 2012.

[50] Wada K, Abass A, Okazaki S, Fukushima Y, Matsunaga H, Tsuzaki K. Fatigue crack threshold of bearing steel at a very low stress ratio. Procedia Struct Integrity 2017;7:391–8. https://doi.org/10.1016/j.prostr.2017.11.104.

[51] Elber W. The significance of fatigue crack closure. Damage tolerance in aircraft structures. ASTM International; 1971.

[52] Murakami Y, Fukuda S, Endo T. Effect of micro-hole on fatigue strength [lst report, effect of micro-hole (dia.: 40, 50, 80, I00 and 200 pm) on the fatigue strength of 0.13% and 0.46% carbon steels]. Trans Jpn Soc Mech Eng Ser I 1978;44(388):4003–13.

[53] Murakami Y, Endo T. The effects of small defects on the fatigue strength of hard steels. Mater, Exper Des Fatigue 1981:431–40.

[54] Yamada K, Kim MG, Kunio T. Tolerant microflaw sizes and non-propagating crack behaviour. EGF1. 1986.

[55] Murakami Y, Toriyama T. Application of the $\sqrt{area}$ parameter model to fatigue strength evaluation of steels containing various artificial defects (holes, cracks and complex defects). Proc 21th Fatigue Symp, SOC Mater Sci Jpn 1992:127–30.

[56] Schönbauer BM, Yanase K, Endo M. The influence of various types of small defects on the fatigue limit of precipitation-hardened 17–4PH stainless steel. Theor Appl Fract Mech 2017;87:35–49. https://doi.org/10.1016/j.tafmec.2016.10.003.

[57] Habib K, Koyama M, Tsuchiyama T, Noguchi H. Fatigue crack non-propagation assisted by nitrogen-enhanced dislocation planarity in austenitic stainless steels. Int J Fatigue 2017;104:158–70. https://doi.org/10.1016/j.ijfatigue.2017.07.019.

[58] Schönbauer BM, Perlega A, Karr UP, Gandy D, Stanzl-Tschegg SE. Pit-to-crack

transition under cyclic loading in 12% Cr steam turbine blade steel. Int J Fatigue 2015;76:19–32. https://doi.org/10.1016/j.ijfatigue.2014.10.010.

[59] Li B, Koyama M, Sakurada E, Yoshimura N, Ushioda K, Noguchi H. Potential resistance to transgranular fatigue crack growth of Fe–C alloy with a supersaturated carbon clarified through FIB micro-notching technique. Int J Fatigue 2016;87:1–5. https://doi.org/10.1016/j.ijfatigue.2016.01.003.

[60] Matsunaga H, Murakami Y, Kubota M, Lee JH. Fatigue strength of Ti-6Al-4V alloys containing small artificial defects. J Soc Mater Sci, Jpn 2003;52(12A ppendix):263–9.

[61] Nisitani H, Endo M. Fatigue strength of carbon steel specimen having an extremely shallow notch (discussion based on successive observation). Trans Jpn Soc Mech Eng 1985;51(464):1008–16.

[62] Nisitani H, Endo M. Unifying treatment of notch effects in fatigue. Trans Jpn Soc Mech Eng Ser I 1985;51:784–9.

[63] Nisitani H, Endo M. Unified treatment of deep and shallow notches in rotating bending fatigue. Basic Questions in Fatigue: Volume I. ASTM International; 1988.

[64] Schönbauer BM, Mayer H. Effect of small defects on the fatigue strength of martensitic stainless steels. Int J Fatigue 2019;127:362–75. https://doi.org/10.1016/j.ijfatigue.2019.06.021.

[65] Wada K. Effects of small defect size and stress ratio on fatigue limit of bearing steel SUJ2 (in Japanese) Bachelor Thesis Japan: Kyushu University; 2015

[66] Chapetti MD, Tagawa T, Miyata T. Ultra-long cycle fatigue of high-strength carbon steels Part II: Estimation of fatigue limit for failure from internal inclusions. Mater Sci Eng, A 2003;356(1–2):236–44. https://doi.org/10.1016/S0921-5093(03)00136-9.

[67] Nisitani H. Size effects of branch point and fatigue limit of carbon steel in rotary bending tests. Trans Jpn Soc Mech Eng A 1968;34(259):371–82.